Journal of Power Sources 224 (2013) 304–311

Contents lists available at SciVerse ScienceDirect

Journal of Power Sources

journal homepage: www.elsevier.com/locate/jpowsour

Evaluation of a cobalt–molybdenum–boron catalyst for hydrogen generation of alkaline sodium borohydride solution–aluminum powder system

Da-Wei Zhuang [a], Qiang Kang [b], Sean S. Muir [c], Xiangdong Yao [c,d], Hong-Bin Dai [a,*], Guang-Lu Ma [a], Ping Wang [a,*]

[a] Shenyang National Laboratory for Materials Science, Institute of Metal Research, Chinese Academy of Sciences, 72 Wenhua Road, Shenyang 110016, PR China
[b] Analysis & Testing Division, Institute of Metal Research, Chinese Academy of Sciences, 72 Wenhua Road, Shenyang 110016, PR China
[c] ARC Centre of Excellence for Functional Nanomaterials, Australian Institute for Bioengineering and Nanotechnology, University of Queensland, Brisbane, QLD 4072, Australia
[d] Queensland Micro- and Nanotechnology Centre, Griffith University, Nathan, QLD 4111, Australia

HIGHLIGHTS

- A newly synthesized Co–Mo–B catalyst is reported.
- The catalyst exhibits remarkably catalytic activity to hydrolysis reaction of $NaBH_4$.
- A hydrogen generation system is composed of $NaBH_4$ solution, catalyst and Al powder.
- This system can yield >6 wt% H_2 with fast kinetics and high fuel conversion.

GRAPHICAL ABSTRACT

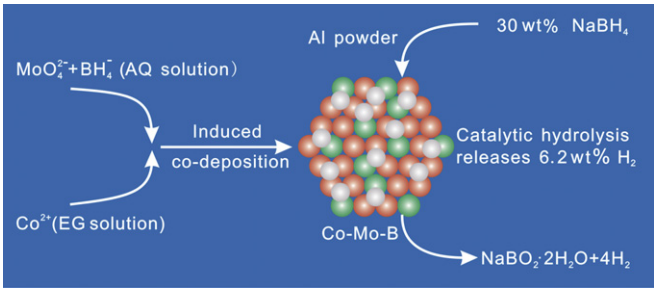

ARTICLE INFO

Article history:
Received 24 July 2012
Received in revised form
25 September 2012
Accepted 27 September 2012
Available online 11 October 2012

Keywords:
Hydrogen generation
Sodium borohydride
Cobalt–molybdenum–boron catalyst
Aluminum powder

ABSTRACT

Catalyst study is a central issue in the development of sodium borohydride ($NaBH_4$)-based hydrogen generation systems. Here, we report the preparation, characterization and utilization of a novel cobalt–molybdenum–boron (Co–Mo–B) catalyst. Our study found that the Co–Mo–B catalyst prepared by chemical reduction method using an ethylene glycol solution of cobalt chloride exhibits remarkably higher catalytic activity than the Co–B and Co–Mo–B catalysts prepared in aqueous solution. On the basis of the phase, microstructure and elemental chemical state analyses, the mechanistic reasons for the improved performance of the newly prepared Co–Mo–B catalyst were discussed. Our study demonstrated that the combined usage of concentrated $NaBH_4$ solution, Co–Mo–B catalyst and a small amount of Al powder constitutes a high-performance hydrogen generation system, which can yield >6 wt% hydrogen with fast kinetics and high fuel conversion.

1. Introduction

The widespread implementation of hydrogen fuel cell technology requires advanced hydrogen storage materials that can store and deliver large amounts of hydrogen at moderate temperatures with fast kinetics. Extensive studies on interstitial metal hydrides and complex hydrides have led to no viable material that can reversibly store over 6 wt% hydrogen at relevant conditions to the practical operation of proton exchange membrane fuel cell [1]. Considerable recent efforts were therefore directed toward the development of H-rich chemical hydrides as potential hydrogen carriers for vehicular and portable applications [2–7].

$$NaBH_4 + (2+x)H_2O \xrightarrow{\text{Catalyst}} NaBO_2 \cdot xH_2O + 4H_2\uparrow + 210\ \text{kJ} \quad (1)$$

Sodium borohydride ($NaBH_4$) is a representative chemical hydride [3–6], which reacts with water to generate H_2 and sodium

* Corresponding authors. Tel.: +86 24 2397 1622; fax: +86 24 2389 1320.
E-mail addresses: hbdai@imr.ac.cn (H.-B. Dai), pingwang@imr.ac.cn (P. Wang).

0378-7753/$ – see front matter © 2012 Elsevier B.V. All rights reserved.
http://dx.doi.org/10.1016/j.jpowsour.2012.09.106

metaborate ($NaBO_2$) following Eqn. (1), where x denotes the number of water of hydration. In the past decade, significant progress has been made in developing $NaBH_4$-based hydrogen generation (HG) system. A number of noble or non-noble transition metals/alloys/salts [8–30] have been identified to be catalytically active toward the hydrolysis reaction of $NaBH_4$. Concurrently, a series of prototype HG generators/systems have been demonstrated that possess power levels ranging from a few watts to kilowatts [9–11,17]. In addition, evolutionary advances have been achieved in regeneration chemistry [31,32], which may potentially allow efficient recycle of spent fuel back to borohydride. But in spite of these technological advances, $NaBH_4$-based HG systems are still limited for vehicular applications [33,34]. This is primarily due to the low effective hydrogen capacity of the system and the prohibitively high hydrogen cost. The former originates from the solubility limitation of $NaBO_2$ in aqueous solution [34,35] and the presence of "dead weight" water of hydration. The latter should be essentially ascribed to the lack of energy-efficient and cost-effective regeneration route [33].

The negative judgment made by US Department of Energy in 2007 [33] frustrated the efforts in developing $NaBH_4$ as a transportation fuel, but it did not extinguish the research interest in the $NaBH_4$-based HG system [34]. Recently, several strategies have been employed to address the key problems of the $NaBH_4$-based HG system. Use of solid $NaBH_4$ to react with water can alleviate the solubility limitation [12,15,36,37], yielding higher hydrogen capacity than the conventional solution-based hydrolysis systems. Combined usage of $NaBH_4$ and aluminum (Al) can effectively improve the HG performance and meanwhile, reduce the hydrogen cost [38–40]. Quite recently, our study further found that using highly active catalyst makes it possible to obtain high hydrogen capacity from the aqueous solution containing high concentration of $NaBH_4$. Since the hydrolysis reaction of $NaBH_4$ is highly exothermic, the rapid proceeding of the hydrolysis reaction will cause rapid temperature rising of the fuel solution, and thereby increasing the solubility of $NaBO_2$ in the aqueous solution.

In the present study, we employed a combination of catalysis and dual-fuel strategies to improve the HG performance of the $NaBH_4$-based system. Our study found that the Co–Mo–B catalyst prepared by a chemical reduction method using an ethylene glycol solution of cobalt chloride ($CoCl_2$) is highly active toward the hydrolysis reaction of $NaBH_4$. Even for a concentrated fuel solution containing 30 wt% $NaBH_4$, the usage of Co–Mo–B catalyst enabled a 100% fuel conversion. When the Co–Mo–B catalyst was used in combination with a small amount of Al powder, the constituted system can rapidly release 6.2 wt% hydrogen within around 5 min. The favorable combination of high hydrogen capacity, fast HG kinetics, high fuel conversion and safe fuel storability, makes the newly developed system very promising for portable hydrogen storage applications.

2. Experimental

2.1. Chemicals and preparation of the catalysts

$NaBH_4$ (96% purity), sodium hydroxide (NaOH, 96%), cobalt chloride hexahydrate ($CoCl_2{\cdot}6H_2O$, 99%) sodium molybdate dihydrated ($Na_2MoO_4{\cdot}2H_2O$, 99%) and ethylene glycol (99%) were purchased from Sinopharm. Al powder (−325 mesh, 99%), Co powder (99.9%), Mo powder (99.9%), CoO powder (95%), MoO_2 powder (99.5%) and MoO_3 powder (99.95%) were purchased from Alfa Aesar. All reagents were used as received. Deionized water was used in preparation of all the aqueous solutions.

The Co–Mo–B catalysts were prepared by chemical reduction method using two solutions: the aqueous or ethylene glycol solution A containing 0.25 M $CoCl_2$; the aqueous solution B containing 1 M $NaBH_4$, 0.25 M NaOH and 0–0.05 M Na_2MoO_4. Here, the concentration of Na_2MoO_4 was varied to adjust the Mo content of the catalyst. The addition of Na_2MoO_4 in solution B instead of solution A was to minimize the formation of MoO_3 precipitate via the reaction between Na_2MoO_4 and $CoCl_2$. In a typical run, 50 mL of solution A was first added in a beaker, followed by dropwise addition of equal volume of solution B using a pressure-equalizing dropping funnel. The solution was kept undisturbed under magnetic stirring until the gas bubbling ceased. After the reaction completed, the black precipitate was magnetically separated from the solution, and then washed thoroughly with deionized water and ethanol to remove the residual Na^+, BH_4^-, BO_2^-, MoO_4^{2-} and Cl^- ions. For comparison, the Co–B catalyst was prepared following the same procedure. The catalyst samples were finally dried at 40 °C under dynamic vacuum for 48 h. The chemical reactions involved in the catalyst preparation process can be described by Eqns. (2)–(5).

$$BH_4^- + 2Co^{2+} + 4OH^- \rightarrow BO_2^- + 2Co\downarrow + 2H_2\uparrow + 2H_2O \quad (2)$$

$$2BH_4^- + 2H_2O \rightarrow 2B\downarrow + 2OH^- + 5H_2\uparrow \quad (3)$$

$$3BH_4^- + 2MoO_4^{2-} + 2H_2O \xrightarrow{Co} 3BO_2^- + 2Mo\downarrow + 6H_2\uparrow + 4OH^- \quad (4)$$

$$BH_4^- + 2H_2O \rightarrow BO_2^- + 4H_2\uparrow \quad (5)$$

2.2. Characterization and HG performance testing

The catalyst samples were characterized by powder X-ray diffraction (XRD, Rigaku D/MAX-2500, Cu $K\alpha$ radiation), transmission electron microscopy (TEM, FEI Tecnai F20) and X-ray photoelectron spectroscopy (XPS, ESCALAB 250, Al $K\alpha$ X-ray source). In preparation of the TEM sample, the catalyst powder was first dispersed in ethanol solution by ultrasound and then deposited on a holey carbon film supported on a copper grid. In the XPS measurements, high-resolution scans of elemental lines were recorded at 50 eV pass energy of the analyzer. All the binding energies were calibrated using the C 1s peak (at 284.6 eV) of the adventitious carbon as an internal standard. The curve fitting was performed using XPS PEAK 4.1 software. After being degassing at 463 K for 12 h, the catalyst samples were measured by N_2 adsorption at 77 K using the Brunauer–Emmett–Teller (BET) method in a Micromeritics ASAP 2010 apparatus to determine the specific surface areas (SSA). Element analyses of the catalyst samples were conducted in an inductively coupled plasma-atomic emission spectrometry (ICP-AES, Iris Intrepid). The magnetization measurements were made in a Quantum Design MPMS-7DC magnetometer under a magnetic field of 0–10,000 Oe at 298 K.

The HG performance testing was conducted in a 250 mL three-neck flask. Unless specified otherwise, the flask was placed in a thermostat that was equipped with a water circulating system to maintain the reaction temperature, typically within ±0.5 °C. In a typical measurement run, the $NaBH_4$ aqueous solution was pre-heated and held at the designated temperature, and then the powdery catalyst attached on a magnetic stirring bar was dropped into the solution to initiate the hydrolysis reaction. In the case of the system using Al powder as additional solid fuel, Al powder was added together with the catalyst. The generated hydrogen gas passed through a trap/heat exchanger to cool to room temperature followed by contacting with a silica drier to remove water vapor.

The HG rate was measured using an online mass flow meter (Seven Star Huachuang, MFM D07–7BM, with an accuracy of ±2%) that was equipped with a computer. The HG volume was calculated by integrating the measured HG rate over time. The reaction temperature was monitored using a thermocouple inserted in the fuel solution and recorded using an online recorder.

3. Results and discussion

3.1. Study of catalytic properties of Co–Mo–B and relevant catalysts

In the present study, we prepared three Co-based catalysts using chemical reduction method. Property examination found that both elemental composition and solvent choice in the preparation process exert profound effects on the catalytic activity of the catalysts. As seen in Fig. 1, the Co–Mo–B catalysts show higher catalytic activity than the Co–B catalyst toward the hydrolysis reaction of $NaBH_4$. Particularly, the Co–Mo–B catalyst that was prepared using an ethylene glycol solution of $CoCl_2$ (denoted as Co–Mo–B (EG) hereinafter) exhibits a remarkably higher activity than the catalyst prepared in aqueous solution (denoted as Co–Mo–B (AQ) hereinafter). The HG kinetics curves all show a nearly linear increase of HG volume with the reaction time, suggesting that the HG from the three systems using different catalysts involve similar reaction mechanisms. Similar quasi-zero-order kinetics was also observed in the $NaBH_4$-based systems with the presence of powdery catalysts [41,42].

Our study found that the catalytic activity of the Co–Mo–B (EG) catalyst can be further improved by properly adjusting the Mo content. Fig. 2 presents the dependence of the HG rate of the catalyzed system on the Mo content of the catalyst. It was found that the Co–Mo–B catalyst containing about 6.4 mol% Mo exhibits the maximum catalytic activity. By using this catalyst, the aqueous solution containing 5 wt% $NaBH_4$ and 5 wt% NaOH can yield H_2 at a rate of 19 L min^{-1} g^{-1} (Co–Mo–B) at 30 °C, which corresponds to a turnover frequency of about 2356 h^{-1} [43]. As seen in Table 1, this stands out as the top level of the known non-noble metal catalysts and is comparable to the performance of noble metal catalysts. The Co–Mo–B catalyst with optimized composition was used in the subsequent studies.

Next, we studied the hydrolysis kinetics of $NaBH_4$ with the presence of the optimized Co–Mo–B catalyst. To minimize the temperature fluctuation of the fuel solution, we conducted the measurements using dilute $NaBH_4$ solution (5 wt% concentration) and reduced the quantity of the catalyst to 5 mg. Fig. 3 gives the HG kinetics curves of the alkaline $NaBH_4$ solution at temperatures ranging from 30 to 50 °C. As expected, the HG rate increases with elevating the solution temperature. In all cases, the catalytic hydrolysis reaction follows zero-order kinetics with respect to $NaBH_4$ concentration. On the basis of the HG rates at the varied temperatures, the apparent activation energy of the hydrolysis reaction of $NaBH_4$ with the presence of Co–Mo–B (EG) catalyst was determined to be 33.3 kJ mol^{-1}. This value compares favorably with the literature results of the Ru/IRA-400 catalyst (47 kJ mol^{-1}) [8], the Co–Cr–B catalyst (37 kJ mol^{-1}) [23], Co–B nanoparticles (43.1 kJ mol^{-1}) [26] and Co–Mo–B catalyst (39 kJ mol^{-1}) [27].

In addition, the newly developed Co–Mo–B catalyst was tested in terms of durability in cyclic usage. After the catalytic hydrolysis reaction, the used catalyst was separated magnetically from the by-product solution, and then washed thoroughly with deionized water for re-usage. The testing results presented in Fig. 4 clearly show the robustness of the Co–Mo–B catalyst. Even at its 10th time usage, the catalyst retained ~90% activity and enabled a 98% fuel

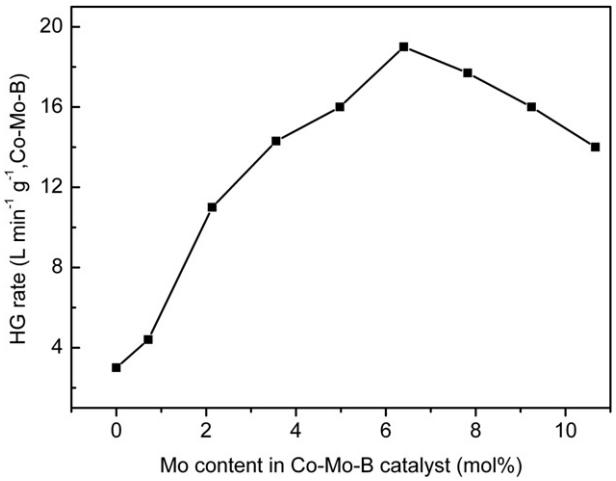

Fig. 2. Effect of Mo content of the Co–Mo–B (EG) catalyst on the HG rate of the system composed of 10 g of 5 wt% $NaBH_4$ + 5 wt% NaOH solution and 20 mg of catalyst at 30 °C.

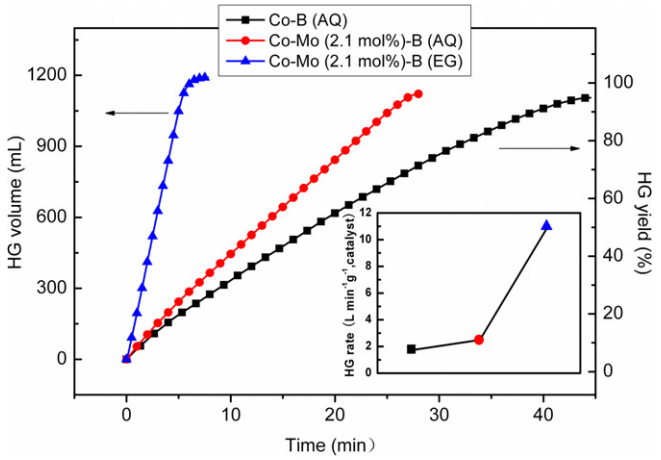

Fig. 1. A comparison of HG kinetics of the system composed of 10 g of 5 wt% $NaBH_4$ + 5 wt% NaOH solution with the presence of 20 mg of difference catalysts at 30 °C. The inset shows the HG rate of the systems using different catalysts.

Table 1
A comparison of the HG rates of the systems using the Co–Mo–B (EG) and other catalysts from open literature.

Catalyst	Reaction condition			HG rate (L min^{-1} g^{-1} cat.)	Ref.
	T (°C)	$NaBH_4$ (wt%)	NaOH (wt%)		
Ru/IRA-400	55	20	10	22	[8]
$Ru_{60}Co_{40}$	25	10	4	17.5	[9]
$Ru_{60}Co_{20}Fe_{20}$	25	10	4	26.8	[9]
Pt/Co_3O_4	25	0.4	–	10.4	[13]
Ni–B	25	1.5	10	0.23	[14]
Co–B	25	20	5	0.88	[18]
Co–W–B/Ni foam	30	20	5	15	[20]
Co/C	20	1	10	10.4	[24]
Co–B/Ni foam	30	20	10	11	[25]
Co–B (EG)	25	3	5	4.93	[26]
Co–Mo–B (AQ)	25	0.1	0.4	2.9	[27]
Co–Mo–Pd–B	25	0.6	5	6.0	[29]
Co–Mo–B (EG)	30	5	5	19	This paper

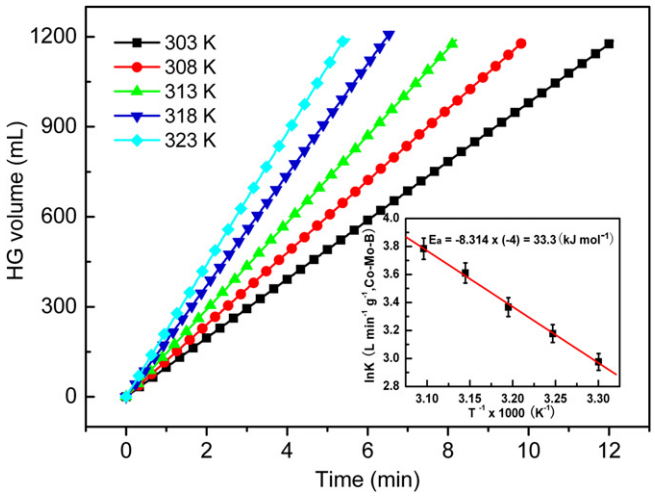

Fig. 3. HG kinetics curves of the system composed of 5 wt% $NaBH_4$ + 5 wt% NaOH solution and 5 mg of Co–Mo–B (EG) catalyst at varied temperatures. The inset shows the Arrhenius treatment of the temperature-dependent HG rate constant (*K*), which determined the apparent activation energy of the hydrolysis reaction of $NaBH_4$ with the presence of Co–Mo–B (EG) catalyst.

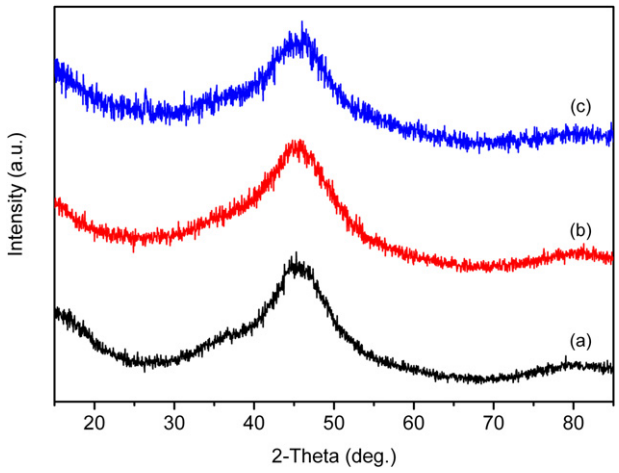

Fig. 5. XRD patterns of the as-prepared (a) Co–B (AQ), (b) Co–Mo–B (AQ) and (c) Co–Mo–B (EG) catalysts.

conversion. The slight degradation in the catalytic activity and fuel conversion should be mainly caused by the loss of the fine catalyst powder during the washing process.

3.2. Characterization of microstructure and element chemical state of Co–Mo–B catalyst

A combination of phase, microstructure and elemental chemical state analyses has been conducted to understand the superior catalytic activity of Co–Mo–B (EG) catalyst, particularly in comparison with the relevant Co–B and Co–Mo–B (AQ) catalysts. Fig. 5 presents the XRD patterns of the as-prepared Co–B (AQ), Co–Mo–B (AQ) and Co–Mo–B (EG) catalysts. All the three catalysts exhibit a broad and featureless peak at around $2\theta = 45^\circ$, indicating their amorphous and/or nanocrystalline structure. A close examination by the HRTEM further found that the catalysts are actually mixtures of nanocrystalline and amorphous phases. As seen in Fig. 6, tiny nanocrystallites with random orientation and a size of 1–5 nm are embedded in an amorphous matrix. According to the selected-area electron diffraction (SAED) results, these nanoparticles should be assigned to metallic Co. This finding agrees well with the literature reports by Geng et al. [44] and Arzac et al. [45]. Their careful studies have elucidated the "core–shell" microstructure of the Ni–B and Co–B catalysts, wherein the multi-component amorphous phases composed of borides and oxides protect the nanocrystalline metallic core from growth and oxidation. This novel microstructure feature may explain the high catalytic activity and long-term stability of the catalysts. But so far no evidence has been obtained to show the microstructure difference among the three catalyst samples that may account for their significantly different catalytic activities.

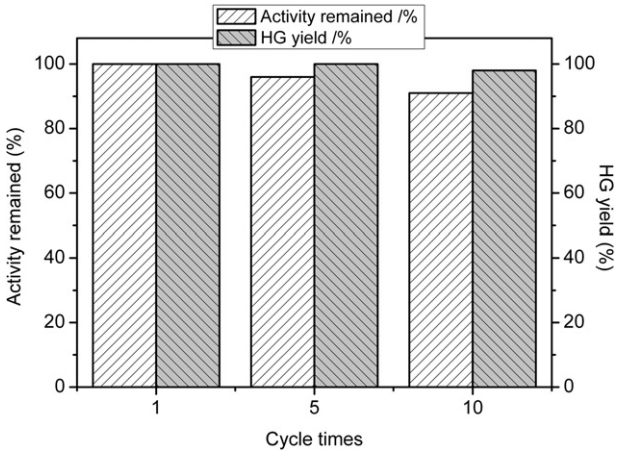

Fig. 4. Cyclic performance of the Co–Mo–B (EG) catalyst in catalyzing the hydrolysis reaction of $NaBH_4$ employing a 10 g of 10 wt% $NaBH_4$ + 5 wt% NaOH solution with the presence of 20 mg catalyst at 30 °C.

Fig. 7 presents the TEM images of the catalyst samples. It was observed that the three catalyst samples showed no substantial difference on the particle sizes, but show decreased agglomeration in the order of Co–B (AQ) > Co–Mo–B (AQ) > Co–Mo–B (EG). This is consistent with the BET results, which determined an increase of SSA in the order of Co–B (AQ) < Co–Mo–B (AQ) < Co–Mo–B (EG), as seen in Table 1. Presumably, the variations of particle agglomeration degree and SSA are associated with the differing magnetism of the catalyst samples. This is supported by the magnetization measurements, which determined the saturation magnetization of the Co–B (AQ), Co–Mo–B (AQ) and Co–Mo–B (EG) catalysts to be 41.1, 37.2 and 34.0 emu g^{-1} (catalyst), respectively. The incorporation of the non-ferromagnetic Mo element causes decline of magnetization property. This may well account for the alleviation of particle agglomeration and increase of SSA of Co–Mo–B catalysts relative to Co–B catalyst. In addition, the ethylene glycol solvent used in the preparation process should also play a stabilizer role in alleviating the particle agglomeration [26]. As a consequence, the Co–Mo–B (EG) catalyst shows larger SSA value than the Co–Mo–B (AQ) catalyst.

Further study found that, besides SSA, elemental chemical state is another possible factor that causes difference in catalytic activity of the catalyst samples. Fig. 8 presents the XPS spectra of three catalysts and the reference samples, from which the binding energy (BE) of the surface elements and likely formed compounds were determined and summarized in Table 2. The as-prepared catalysts exhibit considerable surface oxidation, as evidenced by the clear identification of CoO or $Co(OH)_2$, MoO_2/MoO_3 and B_2O_3 species [27,46–49]. But meanwhile, the signals from metallic Co and Mo remain very strong, which dominate the respective XPS spectra. Among the three constituent elements, Mo is the lightest oxidized one. This is in great contrast to the literature results of the Co–Mo–

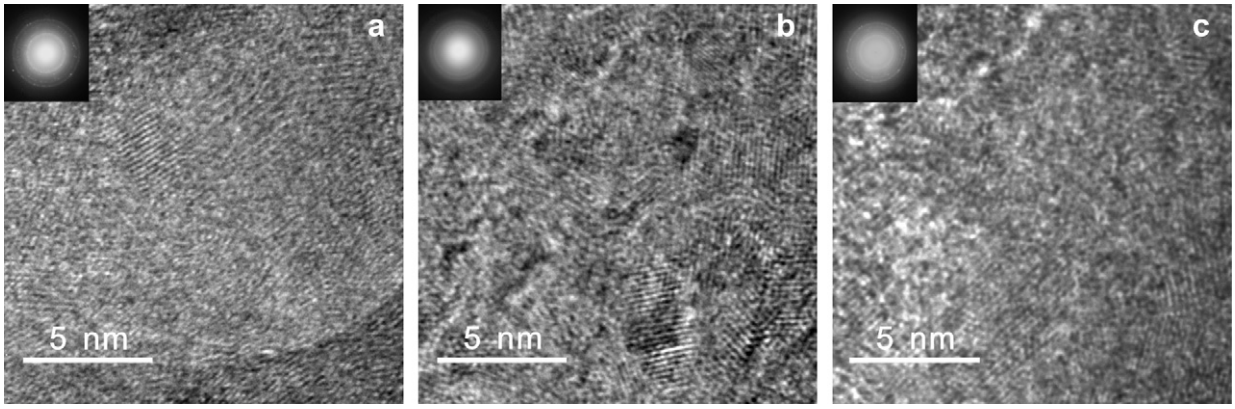

Fig. 6. HRTEM images and SAED patterns of (a) Co–B (AQ), (b) Co–Mo–B (AQ) and (c) Co–Mo–B (EG) catalysts.

B catalyst. According to Chen et al. [48] and Wang et al. [49], the Mo-dopant in their Co–Mo–B catalysts was mainly present in the form of MoO_2/MoO_3. Presumably, the substantial difference in the chemical state of Mo should come from the variation of preparation conditions of the catalyst samples. In the literature works [48,49], the acidic Co^{2+} and alkaline MoO_4^{2-} salts were mixed in the same aqueous solution, resulting in the generation of precipitate in the absence of the complex agent. In contrast, the Co^{2+} and MoO_4^{2-} salts were dissolved in two separate solutions in the present work. When the reaction occurs upon mixing the two solutions, the reduction of metallic Co may induce the co-deposition of metallic Mo [50–52]. Meanwhile, the reaction between Na_2MoO_4 and $CoCl_2$ may also occur, resulting in the formation of MoO_2 and MoO_3. Judging from the relative intensities of the oxidized species in the resolved spectra, the surface oxidation degrees of the Co–Mo–B catalysts are much less than that of the Co–B catalyst. This is another indication of the antioxidation role of elemental Mo. In addition, careful examination of the resolved spectra found that the surface oxidation degree of the Co–Mo–B (EG) catalyst is slightly lower than that of Co–Mo–B (AQ) catalyst. Presumably, this should be attributed to the usage of ethylene glycol in the preparation process, which protects the catalyst surface from oxidation by water. According to the ICP-AES and XPS results (as given in Table 2), the two Co–Mo–B catalysts prepared using different solvents are of quite similar composition. In this case, the reduced surface oxidation generally means increased catalytic activity.

Analysis of the XPS spectra found that the incorporation of Mo into the Co–B catalyst results in small but significant changes of the BEs of the constituent elements. As seen in Fig. 8, the B 1s BE of the Co–B catalyst is positively shifted by 0.9 eV in comparison with the BE of B^0 (187.2 eV) [27,46–49]. But in the Co–Mo–B catalysts, the positive shift of the B 1s BE was reduced to 0.1–0.2 eV. This implies a reduced electron donation from B. Meanwhile, we observed that the Co $2p_{3/2}$ BE is negatively shifted from 778.4 eV for the Co–B catalyst to 777.7–777.8 eV for the Co–Mo–B catalysts, which means an increased electron acceptance from other element(s). A combination of these results clearly suggests that Mo acts as another electron donor in the Co–Mo–B catalysts. This is confirmed by the observed positive shift of Mo $3d_{5/2}$ BE relative to the BE of metallic Mo^0 (227.8 eV) [47]. Careful comparison of the XPS results of the two Co–Mo–B catalysts further found that the Co–Mo–B (EG) catalyst exhibited an increased negative shift of Co $2p_{3/2}$ BE, an increased positive shift of Mo $3d_{5/2}$ BE and a decreased positive shift of B 1s BE relative to the Co–Mo–B (AQ) catalyst. Such BE shifts imply an increased 4d electron transfer from Mo to the vacant d-orbital of Co. According to the classic model proposed by Holbrook and Twist [53], the interaction between the BH_4^- ions and catalyst (M) surface is a key step in the catalyzed hydrolysis of $NaBH_4$. In the resulted M–BH_4^- intermediate complex, the valence electrons of the metal catalyst may enter the antibonding orbital of BH_4^- ions [54], resulting in the weakening of the covalent B–H bond. In this case, increasing the electron density of the active center should facilitate the dissociation of the adsorbed BH_4^-. But on the other hand, overhigh electron density of the catalyst may negatively impact the chemisorption of BH_4^- on the catalyst surface [55]. Therefore, properly tuning the electron density of the

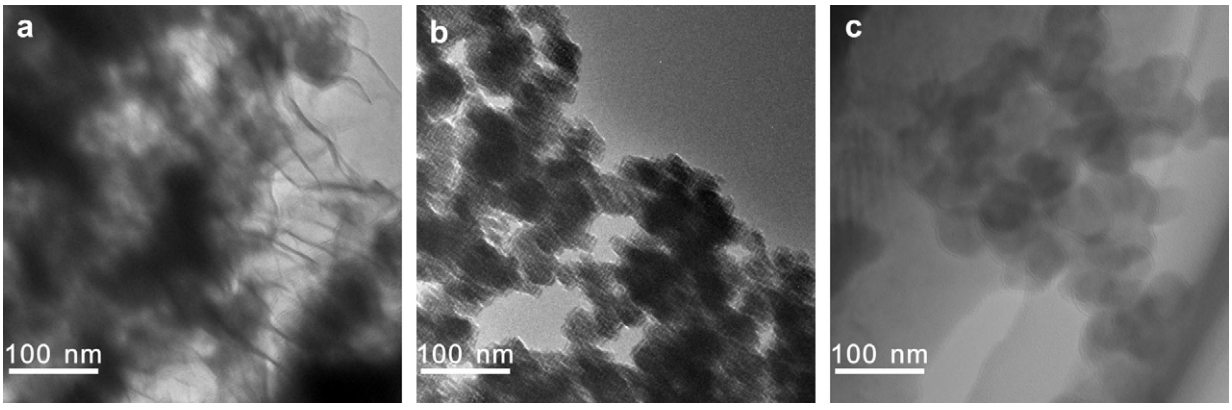

Fig. 7. TEM images of the catalysts: (a) Co–B (AQ); (b) Co–Mo–B (AQ); (c) Co–Mo–B (EG).

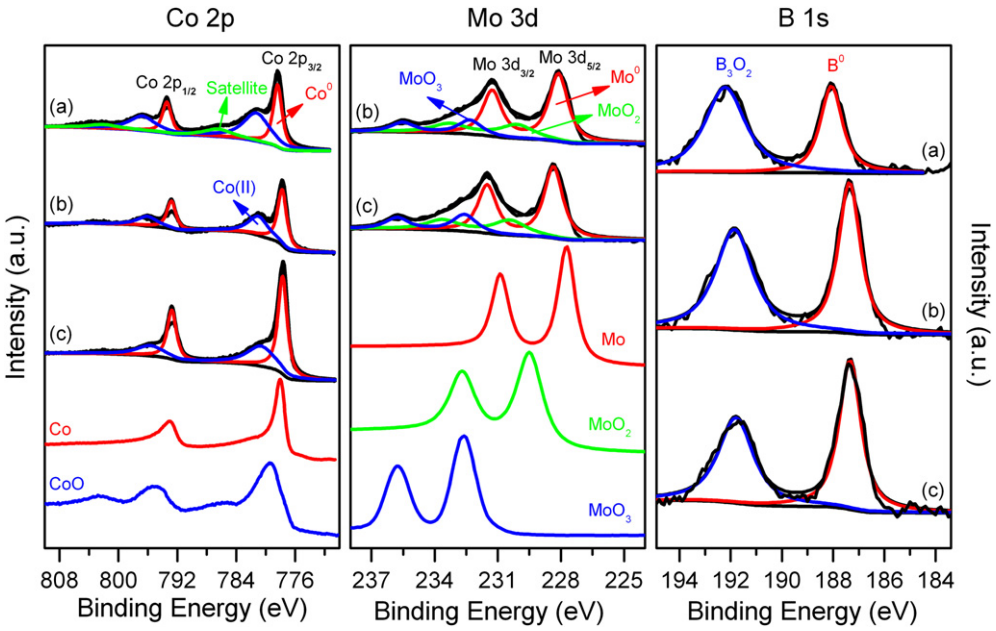

Fig. 8. XPS spectra of the catalyst and reference samples: (a) Co–B (AQ); (b) Co–Mo–B (AQ); (c) Co–Mo–B (EG).

d-band center of the catalyst is crucial for maximizing its catalytic activity. This may provide a possible explanation for the observation of an optimal Mo content in the Co–Mo–B catalyst.

The aforementioned studies suggest that the distinct property advantage of the Co–Mo–B (EG) catalyst over the relevant Co–B (AQ) and Co–Mo–B (AQ) catalysts should be mainly attributed to the modification of electronic structure arising upon incorporation of Mo. In addition, the alleviated particle agglomeration and reduced surface oxidation should also contribute to the superior catalyst activity of the Co–Mo–B (EG) catalyst. But the mechanistic reason(s) for the high intrinsic catalytic activity of the Co–Mo–B (EG) catalyst, particularly the remarkable property difference arising upon changing the solvent in the preparation process remain open questions. In this regard, coupled theoretical and experimental studies are still required.

3.3. Development of high-performance hydrogen generation system using Co–Mo–B (EG) catalyst and Al powder

Low hydrogen capacity is one of the major problems that limit the practical application of $NaBH_4$-based HG systems. Owing to the concern over the solubility limitation of $NaBO_2$, most literature

Table 2
Results of the reference samples and Co–B (AQ), Co–Mo–B (AQ) and Co–Mo–B (EQ) catalysts from XPS, ICP-AES, magnetization and BET measurements.

Sample	Composition (mol%)		Magnetization (emu g^{-1})	S_{BET} (m^2 g^{-1})	Element	Peak BE (eV)	Likely metal/compound
	ICP result	XPS result					
Co powder					Co $2p_{3/2}/2p_{1/2}$	778.0/793.0	Co^0
CoO powder					Co $2p_{3/2}/2p_{1/2}$	779.5/795.3	CoO
						786.4/802.8	
Mo powder					Mo $3d_{5/2}/3d_{3/2}$	227.8/230.9	Mo^0
MoO_2 powder					Mo $3d_{5/2}/3d_{3/2}$	229.5/232.7	MoO_2
MoO_3 powder					Mo $3d_{5/2}/3d_{3/2}$	232.6/235.8	MoO_3
Co–B (AQ)	$Co_{69}B_{31}$	$Co_{65.2}B_{34.8}$	41.1	23.0	Co $2p_{3/2}/2p_{1/2}$	778.4/793.4	Co^0
						781.2/796.7	$CoO/Co(OH)_2$
						786.4/802.2	
					B 1s	188.1	B^0
						192.2	B_2O_3
Co–Mo–B (AQ)	$Co_{65.7}Mo_{5.6}B_{28.7}$	$Co_{58.9}Mo_{6.2}B_{34.9}$	37.2	32.2	Co $2p_{3/2}/2p_{1/2}$	777.8/792.9	Co^0
						781.0/796.5	$CoO/Co(OH)_2$
					Mo $3d_{5/2}/3d_{3/2}$	228.1/231.3	Mo^0
						230.0/233.2	MoO_2
						232.3/235.5	MoO_3
					B 1s	187.4	B^0
						191.9	B_2O_3
Co–Mo–B (EG)	$Co_{62.4}Mo_{6.4}B_{31.2}$	$Co_{58.4}Mo_{6.4}B_{35.2}$	34.0	40.4	Co $2p_{3/2}/2p_{1/2}$	777.7/792.8	Co^0
						780.6/796.1	$CoO/Co(OH)_2$
					Mo $3d_{5/2}/3d_{3/2}$	228.4/231.6	Mo^0
						230.4/233.6	MoO_2
						232.6/235.8	MoO_3
					B 1s	187.3	B^0
						192.1	B_2O_3

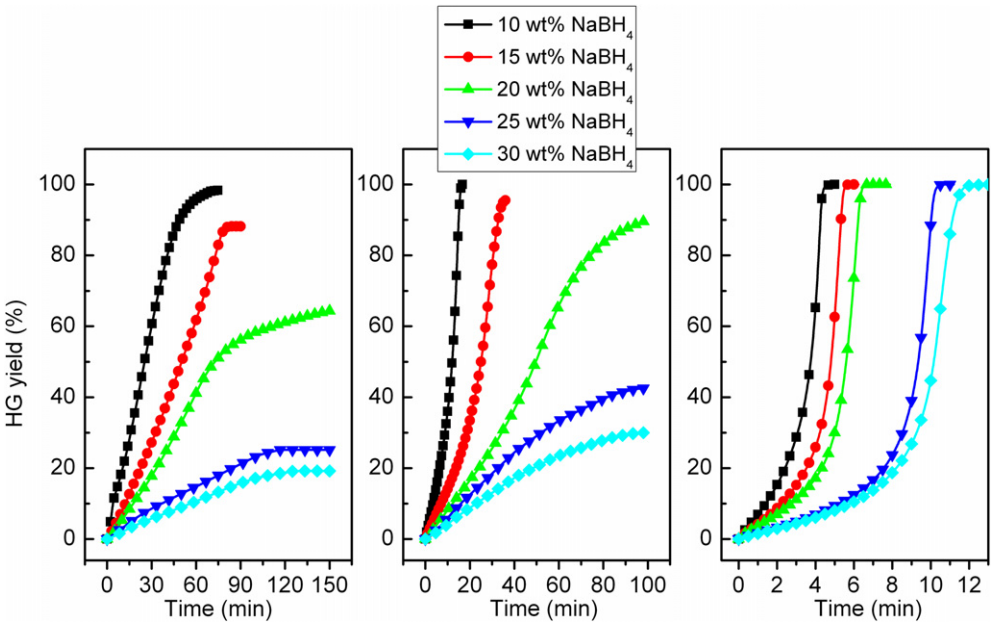

Fig. 9. HG kinetics of the systems composed of 10 g of x wt% $NaBH_4$ + 5 wt% NaOH (x = 10, 15, 20, 25 and 30) aqueous solution with the presence of 20 mg of Co–B (AQ, left), Co–Mo–B (AQ, middle) and Co–Mo–B (EG, right) catalysts, respectively.

reports dealt with dilute fuel solution with a $NaBH_4$ concentration lower than 20 wt% [33,34]. However, our present study showed that it is possible to obtain high hydrogen capacity from concentrated $NaBH_4$ solution by using a highly active catalyst.

Fig. 9 compares the HG performance of the systems with different $NaBH_4$ concentration and with the presence of Co–B (AQ), Co–Mo–B (AQ) and Co–Mo–B (EG) catalysts, respectively. In all the measurements, no attempt was made to control the reaction temperature. It was observed that the systems with a low $NaBH_4$ concentration exhibited fast HG kinetics and high fuel conversion, and increasing the $NaBH_4$ concentration resulted in a degradation of the HG performance. This should be attributed to the solubility limitation of the $NaBO_2$ by-product. With the hydrolysis reaction proceeding, the accumulated borate may cover the surface of the catalyst particles, resulting in the apparent deactivation of the catalyst. Meanwhile, the accumulated by-product may also block the contact of the residual reactant with water, causing serious mass-transfer limitation. But notably, the system employing Co–Mo–B (EG) catalyst exhibited distinct property advantages over the systems catalyzed by the Co–B (AQ) and Co–Mo–B (AQ). Even for the system with a 30 wt% $NaBH_4$ concentration, the usage of Co–Mo–B (EG) catalyst enabled a 100% fuel conversion within 12 min. Here, it should be noted that the applied $NaBH_4$ concentration (30%) is very close to its theoretical value following Eqn. (1) (x = 2), especially after taking the NaOH additive into account. Presumably, this exceptional HG performance should be understood as the combined effects of following aspects: rapid proceeding of the exothermic hydrolysis reaction causes temperature rising of the fuel solution, and thereby increase of the solubility of $NaBO_2$. Vigorous bubbling of H_2 can effectively repel the viscous by-product off the catalyst surface and meanwhile, promote the mass transfer of reactants to the catalyst surface.

The system using concentrated $NaBH_4$ solution has a high hydrogen capacity, but its HG kinetics at early stages is slow. Our study found that this problem can be solved by extra addition of a small amount of Al powder. The rationale behind this approach is the mutual promotion between the hydrolysis reaction of $NaBH_4$ and Al/H_2O reaction [39,40], that is, the alkaline $NaBH_4$ solution can effectively disrupt the passivation layer on the surface of Al and thereby promote the Al/H_2O reaction. As the Al/H_2O reaction is highly exothermic, its proceeding will cause temperature rising of the fuel solution, which in turn promotes the hydrolysis reaction of $NaBH_4$. As seen in Fig. 10, simultaneous addition of Co–Mo–B (EG) catalyst and Al powder to the $NaBH_4$ fuel solution immediately

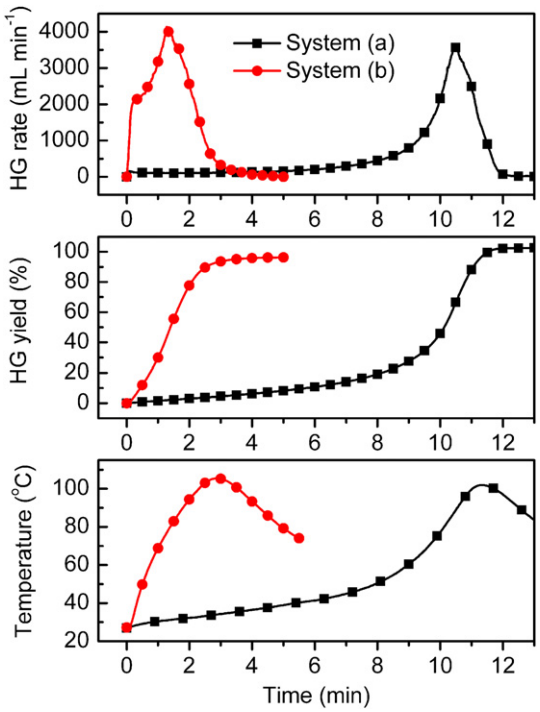

Fig. 10. Comparison of HG rate (top), yield (middle) and reaction temperature (bottom) between the systems: (a) 10 g of 30 wt% $NaBH_4$ + 5 wt% NaOH solution with the presence of 20 mg of Co–Mo–B (EG) catalyst; (b) system (a) with an extra addition of 0.2 g of Al powder.

initiated vigorous H_2 release. The system reached its maximum HG rate of ~4200 mL min^{-1} (corresponding to 210 L min^{-1} g^{-1} catalyst) after 1.3 min, and achieved a 96% fuel conversion within about 5 min. This HG performance is much better than that of the system without Al additive. As an indication and actually a major reason for the kinetics advantage, we observed a much faster temperature rise in the system containing $NaBH_4$ + Al dual fuels relative to the $NaBH_4$-based system. The system composed of 10 g of 30 wt% $NaBH_4$ + 5 wt% NaOH aqueous solution, 0.2 g of Al powder and 20 mg of Co–Mo–B (EG) catalyst yielded a material-based hydrogen capacity of 6.2 wt%. On the basis of the market prices of $NaBH_4$ ($20/kg) and Al ($2.4/kg), the hydrogen production cost of the present system is estimated to be around $100/kg. This is clearly much higher than the US Department of Energy cost target ($2–3/kg). But a favorable combination of high hydrogen capacity, fast HG kinetics, high fuel conversion and safe fuel storability makes the newly developed system promising for portable hydrogen storage applications.

4. Conclusions

A high-performance Co–Mo–B powder catalyst has been prepared by chemical reduction method using an ethylene glycol solution of $CoCl_2$. In comparison with the Co–B and Co–Mo–B catalysts prepared in aqueous solution, the newly synthesized catalyst exhibits remarkably improved catalytic activity toward the hydrolysis reaction of $NaBH_4$. According to a combination of phase, microstructure and elemental chemical state analyses, this property advantage should be understood as combined effects of modified electronic structure arising upon incorporation of Mo, reduced particle agglomeration and alleviated surface oxidation of the catalyst. Owing to its exceptionally high catalytic activity, the Co–Mo–B catalyst can effectively catalyze the hydrolysis reaction of $NaBH_4$ with a concentration as high as 30 wt%. In particular, the combined usage of Co–Mo–B catalyst and a small amount of Al powder enabled rapid, high-yield and high-capacity hydrogen generation from concentrated $NaBH_4$ solution. Our findings are of clear significance for the development of practical $NaBH_4$-based hydrogen generation system for portable applications.

Acknowledgments

The financial supports for this research from the National Basic Research Program of China (973 program, Grant No. 2010CB631305), the National Outstanding Youth Science Foundation of China (Grant No. 51125003), the National Natural Science Foundation of China (Grant No. 51071155) and the Natural Science Foundation of Liaoning Province (Grant No. 20102231) are gratefully acknowledged.

References

[1] L. Schlapbach, Nature 460 (2009) 809–811.
[2] P. Wang, X.D. Kang, Dalton Trans. (2008) 5400–5413.
[3] B.H. Liu, Z.P. Li, J. Power Sources 187 (2009) 527–534.
[4] S.S. Muir, X.D. Yao, Int. J. Hydrog. Energy 36 (2011) 5983–5997.
[5] D.M.F. Santos, C.A.C. Sequeira, Renew. Sustain. Energy Rev. 15 (2011) 3980–4001.
[6] U.B. Demirci, O. Akdim, J. Andrieux, J. Hannauer, R. Chamoun, P. Miele, Fuel Cells 10 (2010) 335–350.
[7] J. Wang, X.-B. Zhang, Z.-L. Wang, L.-M. Wang, Y. Zhang, Energy Environ. Sci. 5 (2012) 6885–6888.
[8] S.C. Amendola, S.L. Sharp-Goldman, M.S. Janjua, M.T. Kelly, P.J. Petillo, M. Binder, J. Power Sources 85 (2000) 186–189.
[9] J.H. Park, P. Shakkthivel, H.J. Kim, M.K. Han, J.H. Jang, Y.R. Kim, H.S. Kim, Y.G. Shue, Int. J. Hydrog. Energy 33 (2008) 1845–1852.
[10] Q. Zhang, G. Smith, Y. Wu, R. Mohring, Int. J. Hydrog. Energy 31 (2006) 961–965.
[11] Y. Kojima, K. Suzuki, K. Fukumoto, Y. Kawai, M. Kimbara, H. Nakanishi, S. Matsumoto, J. Power Sources 125 (2004) 22–26.
[12] Y. Kojima, Y. Kawai, H. Nakanishi, S. Matsumoto, J. Power Sources 135 (2004) 36–41.
[13] T.F. Hung, H.C. Kuo, C.W. Tsai, H.M. Chen, R.S. Liu, B.J. Weng, J.F. Lee, J. Mater. Chem. 21 (2011) 11754–11759.
[14] D. Hua, Y. Hanxi, A. Xinping, C. Chuansin, Int. J. Hydrog. Energy 28 (2003) 1095–1100.
[15] M.J.F. Ferreira, C.M. Rangel, A.M.F.R. Pinto, Int. J. Hydrog. Energy 37 (2012) 6985–6994.
[16] K. Kim, T. Kim, K. Lee, S. Kwon, J. Power Sources 196 (2011) 9069–9075.
[17] G.M. Arzac, A. Fernández, A. Justo, B. Sarmiento, M.A. Jiménez, M.M. Jiménez, J. Power Sources 196 (2011) 4388–4395.
[18] S.U. Jeong, R.K. Kim, E.A. Cho, H.J. Kim, S.W. Nam, I.H. Oh, S.A. Hong, S.H. Kim, J. Power Sources 144 (2005) 129–134.
[19] U.B. Demirci, P. Miele, Phys. Chem. Chem. Phys. 12 (2010) 14651–14665.
[20] H.B. Dai, Y. Liang, P. Wang, X.D. Yao, T. Rufford, M. Lu, H.M. Cheng, Int. J. Hydrog. Energy 33 (2008) 4405–4412.
[21] R. Fernandes, N. Patel, A. Miotello, Int. J. Hydrog. Energy 34 (2009) 2893–2900.
[22] N. Patel, A. Miotello, V. Bello, Appl. Catal. B Environ. 103 (2011) 31–38.
[23] R. Fernandes, N. Patel, A. Miotello, Appl. Catal. B Environ. 92 (2009) 68–74.
[24] J. Zhu, R. Li, W.L. Niu, Y.J. Wu, X.L. Gou, J. Power Sources 211 (2012) 33–39.
[25] H.B. Dai, Y. Liang, P. Wang, H.M. Cheng, J. Power Sources 177 (2008) 17–23.
[26] Z. Wu, S. Ge, Catal. Commun. 13 (2011) 40–43.
[27] N. Patel, R. Fernandes, A. Miotello, J. Catal. 271 (2010) 315–324.
[28] R. Fernandes, N. Patel, A. Miotello, R. Jaiswal, D.C. Kothari, Int. J. Hydrog. Energy 36 (2011) 13379–13391.
[29] Y. Zhao, Z. Ning, J. Tian, H. Wang, X. Liang, S. Nie, Y. Yu, X. Li, J. Power Sources 207 (2012) 120–126.
[30] H.I. Schlesinger, H.C. Brown, A.E. Finholt, J.R. Gilbreath, H.R. Hoekstra, E.K. Hyde, J. Am. Chem. Soc. 75 (1953) 215–219.
[31] Y. Kojima, T. Haga, Int. J. Hydrog. Energy 28 (2003) 989–993.
[32] D.L. Calabretta, B.R. Davis, J. Power Sources 164 (2007) 782–791.
[33] Go/No-Go Recommendation for Sodium Borohydride for On-Board Vehicular Hydrogen Storage, U.S. Department of Energy Hydrogen Program, Independent Review, Nov. 2007.http://www.hydrogen.energy.gov/pdfs/42220.pdf.
[34] U.B. Demirci, O. Akdim, P. Miele, Int. J. Hydrog. Energy 34 (2009) 2638–2645.
[35] Y. Shang, R. Chen, Energy Fuels 20 (2006) 2142–2148.
[36] B.H. Liu, Z.P. Li, S. Suda, J. Alloy. Compd. 468 (2009) 493–498.
[37] C.H. Liu, Y.C. Kuo, B.H. Chen, C.L. Hsueh, K.J. Hwang, J.R. Ku, F.H. Tsau, M.S. Jeng, Int. J. Hydrog. Energy 35 (2010) 4027–4040.
[38] E. Shafirovich, V. Diakov, A. Varma, Combust. Flame 144 (2006) 415–418.
[39] H.-B. Dai, G.-L. Ma, H.-J. Xia, P. Wang, Fuel Cells 11 (2011) 424–430.
[40] H.B. Dai, G.L. Ma, X.D. Kang, P. Wang, Catal. Today 170 (2011) 50–55.
[41] H.B. Dai, Y. Liang, L.P. Ma, P. Wang, J. Phys. Chem. C 112 (2008) 15886–15892.
[42] J. Andrieux, U.B. Demirci, P. Miele, Catal. Today 170 (2011) 13–19.
[43] Turnover frequency (TOF) is calculated using the following equation: TOF = The amount of products (mol)\(The amount of the catalyst active sites (mol) × Time (h)). Here, the Co–Mo–B catalyst with a composition of $Co_{62.4}Mo_{6.4}B_{31.2}$ has a molar mass of 46.3 g mol^{-1}.
[44] J. Geng, D.A. Jefferson, B.F.G. Johnson, Chem. Commun. (2007) 969–971.
[45] G.M. Arzac, T.C. Rojas, A. Fernández, ChemCatChem 3 (2011) 1305–1313.
[46] S. Cavaliere, J. Hannauer, U.B. Demirci, O. Akdim, P. Miele, Catal. Today 170 (2011) 3–12.
[47] C.D. Wagner, W.M. Riggs, L.E. Davis, J.F. Moulder, G.E. Mulenberg (Eds.), Handbook of X-ray Photoelectron Spectroscopy, first ed. Perkin Elmer Corporation, 1979.
[48] X. Chen, H. Li, H. Luo, M. Qiao, Appl. Catal. A-Gen. 233 (2002) 13–20.
[49] W. Wang, Y. Yang, H. Luo, T. Hu, W. Liu, Catal. Commun. 12 (2011) 436–440.
[50] A. Brenner, Electrodeposition of Alloys, vol. II, Academic Press, New York and London, 1963, p. 429.
[51] E.J. Podlaha, D. Landolt, J. Electrochem. Soc. 144 (1997) 1672–1680.
[52] N. Petrov, Y. Sverdlov, Y. Shacham-Diamand, J. Electrochem. Soc. 149 (2002) C187–C194.
[53] K.A. Holbrook, P.J. Twist, J. Chem. Soc. A (1971) 890–894.
[54] M.C.S. Escaño, E. Gyenge, R.L. Arevalo, H. Kasai, J. Phys. Chem. C 115 (2011) 19883–19889.
[55] J.K. Nørskov, T. Bligaard, J. Rossmeisl, C.H. Christensen, Nat. Chem. 1 (2009) 37–46.